

See discussions, stats, and author profiles for this publication at: <https://www.researchgate.net/publication/229478602>

Remarkable Stability of High Energy Conformers in Self-Assembled Monolayers of a Bistable Electro-and Photoswitchable Overcrowded Alkene

ARTICLE *in* THE JOURNAL OF PHYSICAL CHEMISTRY C · NOVEMBER 2011

Impact Factor: 4.77 · DOI: 10.1021/jp206889y

CITATIONS

9

READS

98

10 AUTHORS, INCLUDING:



Oleksii Ivashenko

University of Alberta

18 PUBLICATIONS 167 CITATIONS

[SEE PROFILE](#)



Hella Logtenberg

University of Groningen

8 PUBLICATIONS 100 CITATIONS

[SEE PROFILE](#)



Petra Rudolf

University of Groningen

256 PUBLICATIONS 5,688 CITATIONS

[SEE PROFILE](#)



Wesley R Browne

University of Groningen

209 PUBLICATIONS 4,736 CITATIONS

[SEE PROFILE](#)

Remarkable Stability of High Energy Conformers in Self-Assembled Monolayers of a Bistable Electro- and Photoswitchable Overcrowded Alkene

Oleksii Ivashenko,[†] Hella Logtenberg,[‡] Jetsuda Areephong,[‡] Anthony C. Coleman,[‡] Philana V. Wesenhausen,[‡] Edzard M. Geertsema,[‡] Nicolas Heureux,[‡] Ben L. Feringa,^{*,†,‡} Petra Rudolf,^{*,†} and Wesley R. Browne^{*,†}

[†]Zernike Institute for Advanced Materials and [‡]Stratingh Institute for Chemistry, University of Groningen, Nijenborgh 4, 9747 AG Groningen, The Netherlands

 Supporting Information

ABSTRACT: Although bistability of molecular switches in solution is well established, achieving highly robust bistable molecular switching in self-assembled monolayers remains a challenge. Such systems are highly attractive as components in organic electronics and molecular-based photo and electrochromic devices. Here we report a remarkably robust surface confined bithiaxanthylidene redox switch that shows excellent bistability, manifested in reversible changes in spectroscopic and electrochemical properties and in physical properties such as water contact angle changes (ca. 30° difference in water contact angle between the two redox states of a bithiaxanthylidene self-assembled monolayer). The effect of surface immobilization of bithiaxanthylidene on its photochromic, thermal and electrochemical properties is described. Surface immobilization is achieved by incorporating thiol- and alkylsiloxy-terminated “legs” on one of the tricyclic aromatic units. The molecular switch in its neutral and dicationic state, generated by bulk electrolysis, was characterized in solution, in the solid state and on surfaces, by UV/vis absorption, Fourier transform infrared, X-ray photoelectron, and Raman spectroscopies and by cyclic voltammetry. In solution, the redox switching to the dicationic state is achieved by oxidation at 1.2 V versus SCE. Reduction of the dication at <0.4 V results in initial formation of a highly unstable twisted conformation that reverts via a *syn*-folded conformational state to the most stable (*anti*-folded) conformer. Although the *syn*-folded state can be obtained by UV irradiation at <0 °C, the twisted conformation is not observable in solution, even at 200 K. Remarkably, in monolayers on electrodes this highly unstable form (which is generated by reduction of the dicationic state) is relatively stable even for several minutes. This stability is ascribed to the formation of densely packed monolayers in which the intermolecular interactions provide for a substantial barrier to thermal interconversion of the various conformational states.



INTRODUCTION

Bringing molecular bistability from solution to surfaces is without doubt one of the most exciting challenges in molecular switching currently, not least because of the potential to control surface properties with external stimuli such as light and redox reactions.¹ Such “smart” surfaces, that is, surfaces that are stimuli responsive, hold considerable potential for application in areas as diverse as organic electronics,² magnetic memory³ and logic,⁴ biocompatibility, and cell culture on surfaces.⁵ Achieving robust bistability, under repeated operation, either photo- or electrochemically, is essential for real applications and ideally a large hysteresis in the switching and thermal bistability is preferable, as is key to magnetic memory, for example, in the light-induced spin crossover systems.⁶ In this regard, the structurally simple overcrowded alkene bithiaxanthylidene is an excellent candidate for redox control of surface properties due to its fascinating photochemically, thermally, and redox-driven switching behavior.⁷

The photochemical, thermal, and electrochemical properties and the dynamic stereochemistry⁸ of overcrowded alkenes⁹ have captured the imagination of chemists for over 100 years.¹⁰ Over

the last decade, this class of functional compounds has seen application in the development of functional molecular materials, molecular switches, and devices. Most notable are the bistricyclic aromatic enylidenes (BAE)¹¹ and phenanthrylidenes¹² that were the basis for unidirectional light-driven molecular motors.^{12b,d}

The thermal and photochemical properties of BAEs are highly sensitive to variations in molecular structure.^{13,14} Indeed, even structurally simple BAEs show complex thermo-, photo-, and electrochromic behavior, such as the bithiaxanthylidene **1**, for which we reported recently the unprecedented three-state-switching of luminescence between blue, red, and nonfluorescent states using a combination of electrochemical, photochemical, and thermal stimuli (Scheme 1).⁷

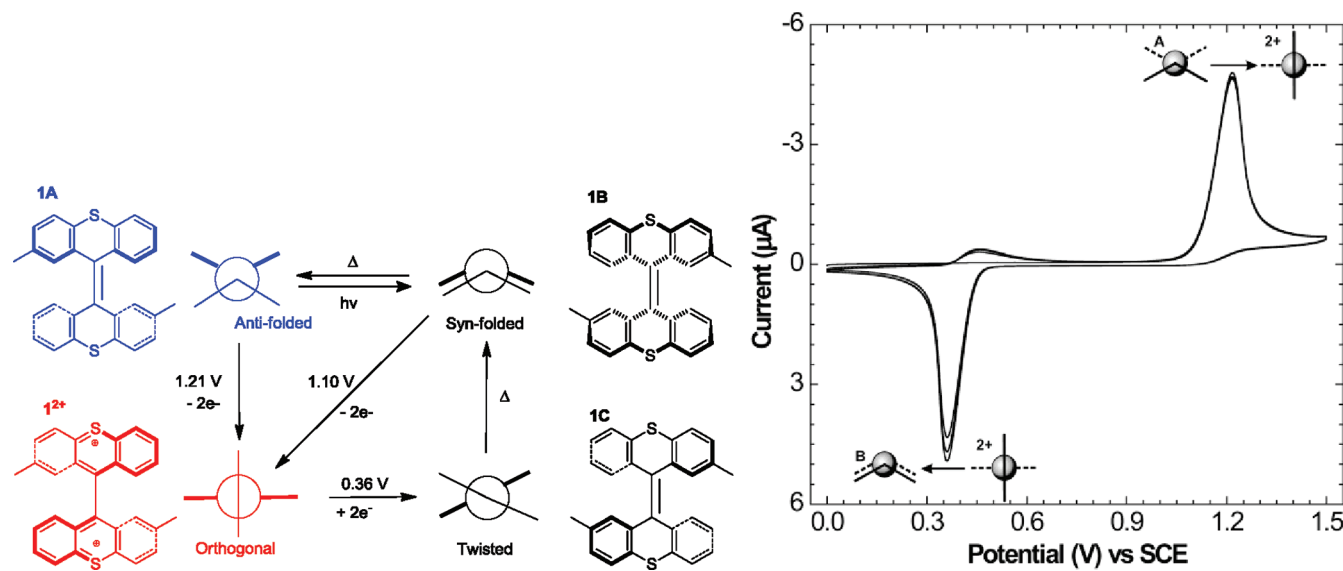
The overcrowded alkene dimethyl-bithiaxanthylidene (**1**) can adopt any of three distinct conformational states, *anti*-folded (**1A**), *syn*-folded (**1B**), and twisted (**1C**); with the *anti*-folded

Received: July 19, 2011

Revised: October 6, 2011

Published: October 10, 2011

Scheme 1. Interconversion between the Three Conformers of **1** (**1A–1C**) and the Oxidized State **1²⁺** is Driven by a Combination of Light, Heat and Electrochemical Oxidation/Reduction^a



^a Only *trans*-isomers are shown for clarity (left). Upon oxidation and reduction the change in conformation results in a 0.85 V hysteresis in the cyclic voltammogram (right, thin-layer CV, scan rate 0.1 V s⁻¹, glassy carbon electrode, initial potential is 0.0 V).⁷ The changes in molecular structure that accompany each redox process are shown schematically.

(**1A**) conformation being the most thermodynamically favorable and the only conformation observed at 293 K in solution. Previously we have demonstrated that switching between the various conformational states can be achieved by the interplay of external stimuli, that is, applied potential (electrochemical switching), temperature (thermal switching), and light (photochromic switching), Scheme 1.⁷ The metastable *syn*-folded conformer (**1B**) can be obtained from **1A** either by UV irradiation or an electrochemical oxidation/reduction cycle at temperatures below 0 °C.⁷ The twisted conformer (**1C**) is too unstable for a significant population to be maintained even at 200 K in solution. The bisthioxanthylum dication (**1²⁺**), which is obtained from **1A** by a two-electron oxidation, can be isolated, using bulk electrolysis, as a stable red solid and has been characterized by single crystal X-ray structural analysis.⁷ The structure of **1²⁺** is analogous to **1C** with the upper and lower tricyclic groups orientated orthogonally with respect to each other (Scheme 1).

Such a wide range of functionality, and excellent redox and photochemical robustness, in a single molecular species is a rather unique and highly attractive feature with regard to the preparation of responsive molecularly modified surfaces. This raises an important question: Can the switching properties in solution be reproduced when immobilized on a surface and does surface immobilization influence the rates of the transformations between the various states?

The importance of intermolecular interactions upon surface confinement was highlighted recently by our group for a related blue fluorescent BEA in which the upper half contained a sulfur atom and the lower half a methylene unit.¹⁵ In that case, the compound underwent a 6-π electron pericyclic ring closing reaction followed by rapid irreversible dehydrogenation in the presence of molecular oxygen to form a photostable green fluorescent compound.¹⁶ Immobilization of this irreversibly switchable blue fluorescent BEA on quartz and ITO surfaces, however,

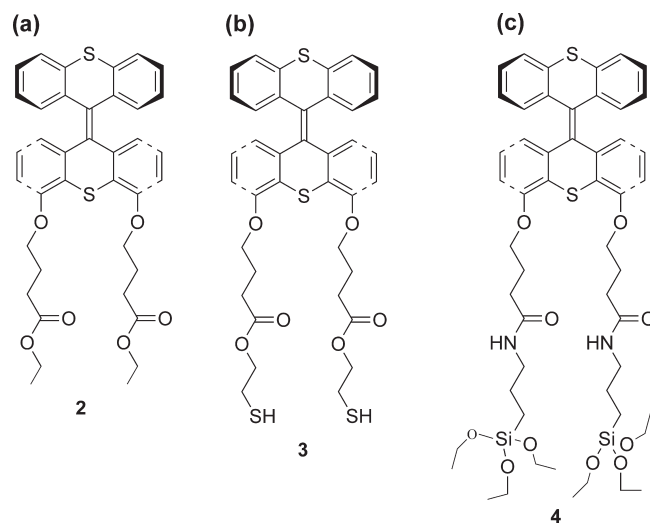


Figure 1. Structures of compounds used in this study: (a) model compound **2** used to compare properties in solution with those observed on surfaces, compounds (b) **3** and (c) **4** used to form self-assembled monolayers on gold and monolayers on ITO and quartz, respectively.

led to the isomerization being inhibited by intermolecular energy transfer quenching. Such quenching was not observed in solution. In this case, the effect of immobilization of the photochrome as a monolayer on a surface was to change the kinetic competitiveness of the various excited state deactivation pathways compared with those observed in solution.⁷

For the overcrowded alkenes described here, such as **2–4A** (see Figure 1), the large structural changes that accompany both photochemical and redox switching could give rise to cooperative or inhibitory effects at high packing densities when immobilized on surfaces as monolayers. Furthermore, the proximity of

molecules in a monolayer can profoundly influence the kinetics of inter- and intramolecular reactions including rates of disproportionation¹⁷ and energy transfer quenching.¹⁵ Because of the large structural changes involved upon electrochemical switching, it can be expected¹⁸ that, in the closely packed environment of a self-assembled monolayer (SAM), intermolecular interactions will modify the conformational properties of the compound and allow for the observation of highly conformational unstable species such as the twisted isomer **2–4C** (Scheme 1).

In the present contribution the effect of immobilization of analogs of **1**, which are based on the same BAE core but with two ‘legs’ for surface attachment, is investigated on a range of surfaces, with regard to changes in electrochemical, thermal and photochemical behavior. Modification of the overcrowded alkene with thiol- or alkylsiloxy-terminated aliphatic “legs” enables immobilization of the overcrowded alkenes (**3** and **4**) on gold, quartz, and ITO surfaces (Figure 1), a strategy employed recently for a range of related overcrowded alkenes, especially the light-driven molecular rotary motors.¹⁹ The goal is to understand how packing in a SAM can be used to tune molecular properties beyond what is achievable with modifications in molecular structure. This aspect could open up new opportunities in the application of organic materials in organic electronics by generating functions and complex responses of surfaces to external stimuli.

■ EXPERIMENTAL SECTION

All chemicals were purchased from commercial sources (Sigma Aldrich, Acros) and used as received without further purification unless stated otherwise. All solvents used for spectroscopic and electrochemical measurements were Uvasol grade (Merck) unless stated otherwise. Details for the synthesis and characterization of all compounds and procedures for the preparation of surfaces used are available as Supporting Information.

Monolayer Preparation. For XPS, vibrational and absorption spectroscopy, spectroelectrochemistry, ellipsometric, and contact angle measurements, samples were prepared by self-assembly from a 10^{-4} M solution of **3** in dichloromethane or ethanol. Freshly prepared gold surfaces were immersed in a solution of **3** overnight at room temperature in the dark. Quartz and ITO slides were functionalized with **4** by heating at reflux in toluene overnight. After functionalization of the surface, the substrate was rinsed with ethanol and dichloromethane, thoroughly dried with an argon gas stream, and introduced immediately into the measuring system. Thin films of **2A** and **2²⁺** for XPS measurements were prepared by dropcasting on a gold substrate using CHCl₃ and CH₃CN solutions, respectively.

Ellipsometric Measurements. The thickness of the film on a surface was determined using a VASE ellipsometer VB-400 (J. A. Woolam Co., Inc.) with a control module unit, a high speed monochromator system HS-190, and 75 W light source. The system was calibrated on a silicon wafer, and a fresh 150 nm thick gold on mica reference substrate was used to generate the mathematical model used to calculate film thickness.²⁰

Contact Angle Measurements. Contact angles were measured on a Device Dataphysics instrument with SCA20, version 3.60.2, software. A 2 μ L drop of doubly distilled deionized water was used as the measuring liquid (sessile drop method). A minimum of five spots on each sample were probed and the contact angles averaged. Analysis consisted of applying a baseline and elliptical curve fitting of the water–air contact profile. The uncertainty in the measurements is $\pm 3^\circ$.

X-ray Photoelectron Spectroscopy (XPS). XPS was performed using a Surface Science SSX-100 ESCA instrument. The pressure in the measurement chamber was maintained below 10^{-10} mbar during data acquisition. The spectrometer is equipped with a monochromatic Al K α X-ray source ($h\nu = 1486.6$ eV). The electron takeoff angle with respect to the normal to the surface was 37° . To verify that the monolayer formed on a substrate is homogeneous and uniform and to minimize X-ray induced degradation, spectra were collected at a minimum of four different spots on the sample. Data were checked for consistency and averaged for each spectral interval. The spot diameter of the analyzed area was $1000 \mu\text{m}$ with a spectral resolution of 1.26 eV (or 1.67 eV for a broad survey scan). The measurement started with the sulfur S2p and carbon C1s regions, as they are the most prone to X-ray damage,²¹ and then oxygen O1s and gold Au4f regions, a survey scan was taken also. XPS spectra were analyzed using the least-squares curve fitting program Winspec.²² Binding energies are reported ± 0.1 eV and referenced to the Au 4f_{7/2} photoemission peak originating from the substrate, centered at a binding energy of 84 eV.²³ Deconvolution of spectra included Shirley²⁴ baseline subtraction and fitting with a number of peaks consistent with the structure of the molecules on a surface, taking the experimental resolution into account. The profile of the peaks was taken as a convolution of Gaussian and Lorentzian functions. Quantitative analysis was performed taking into account the sensitivity factors for each element specific to the spectrometer used. The uncertainty in the peak intensity determination is 4% for sulfur and 1% for carbon, gold, and oxygen. The thickness of the molecular layer was estimated using the assumption of an attenuation length of 42 Å, as reported for SAMs of alkane thiols on gold.²⁵

Electrochemical Measurement. Electrochemical measurements were performed using either a CHInstruments 600C or 760C potentiostat. A three-electrode arrangement with a reference electrode (Hg/HgSO₄, Ag/AgCl wire pseudo-reference electrode or SCE), Pt wire auxiliary electrode and glassy carbon, gold or ITO working electrode was used. The electrolyte was a freshly prepared 0.1 M solution of tetrabutylammonium hexafluorophosphate (TBAPF₆, Sigma Aldrich Co, electrochemical grade) in acetonitrile or dichloromethane.²⁶ All potentials are reported with respect to the Saturated Calomel Electrode (SCE). Redox potentials are reported ± 10 mV. The surface coverage of the electrodes by **3** and **4** was determined from the reduction peak on the first or second sweep, taking into account the area of the electrode obtained by the AuO reduction wave measured in 1 N H₂SO₄ prior to monolayer deposition and measuring the geometric area of the electrode, respectively. Capacitance of the double layer at the electrode was determined from the scan-rate dependence of the non-Faradic current (within a potential range removed from redox processes of **3** or **4**) in TBAPF₆ in acetonitrile.

Vibrational and Electronic Absorption Spectroscopy. Infrared spectra were collected on Perkin-Elmer FT-IR Spectrometer “Spectrum 400” using a UATR attachment and liquid N₂ cooled MCT detector. Raman spectra were recorded at 785 nm using a Perkin-Elmer Raman Station 400F. The spot size for Raman measurements was $100 \mu\text{m}^2$. Raman spectra were recorded typically with 4–5 exposures of 5–10 s duration. Further analysis of the Raman spectra involved manual baseline correction and subtraction of the solvent signal where appropriate. UV-vis absorption spectra were obtained using either a JASCO V630 or an Analytik Jena Specord S600 diode array spectrophotometer. Semitransparent substrates of 20 nm Au on

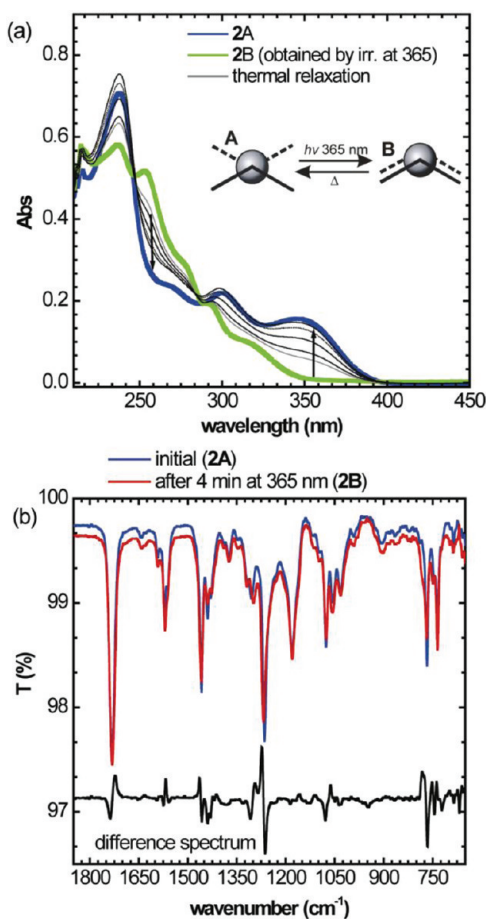


Figure 2. (a) Conversion of **2A** (blue) to **2B** (green) in solution at 273 K by irradiation at 365 nm followed by the thermal recovery of **2A** over 10 min (indicated by arrows) monitored by UV/vis absorption spectroscopy and (b) FTIR spectrum of **2A** in the solid state at 293 K before (blue) and after (red) irradiation at 365 nm; the difference spectrum (black) is shown offset.

glass with a 2 nm Cr interlayer, ITO, or quartz slides were used. Photochemical switching was achieved using a Spectroline 365 nm (center wavelength) lamp.

Raman and UV/vis spectroelectrochemistry were obtained as described above with a CHI600c potentiostat with Ag/AgCl reference electrode, Pt auxiliary electrode, and either a platinum gauze, in the case of **2**, or a roughened gold bead with a monolayer of **3** as a working electrode.

RESULTS AND DISCUSSION

The synthesis and NMR and MS characterization of compounds **2–4** are provided as SI. Briefly, a divergent strategy was employed where the anchor groups in the case of **3** and **4** or an ester group in the case of **2** were attached in the final step. The ¹H NMR, FTIR, and Raman spectra of compounds **2** and **3** (see SI, Figures S1–3) confirm that the peripheral difference between the two compounds has little, if any, effect on the structure of the BAE unit. **2²⁺** was prepared by electrochemical oxidation and isolated as described for **1²⁺** earlier (see SI).⁷

Photo- and Electrochemistry of **2 and **2²⁺** in Solution.** The approach taken to immobilize the bisthianthylidene (**1**) on electrode surfaces, that is, by attaching alkoxy “legs” to one-half of

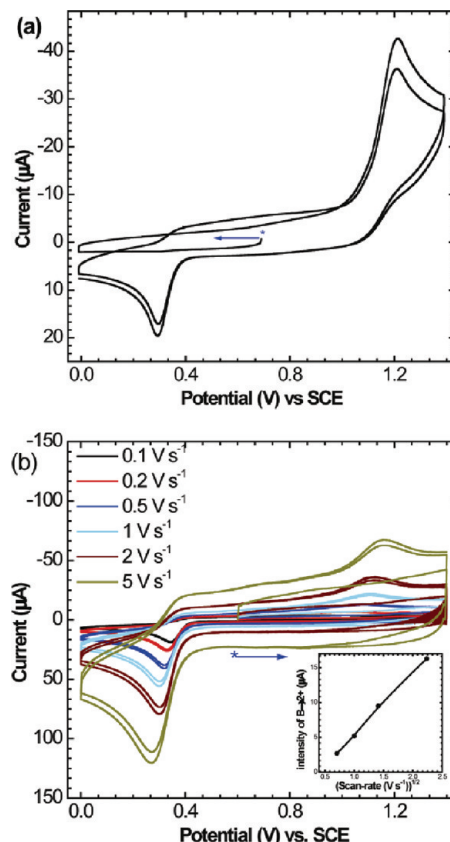


Figure 3. Cyclic voltammetry of a glassy carbon electrode (a) **2A** and (b) **2²⁺(PF₆)₂** (inset: current vs $\sqrt{\text{scan rate}}$) in CH_2Cl_2 (0.1 M TBAPF₆). The initial potential and initial scan directions are indicated by an “*” and an arrow, respectively.

the molecule, requires that a more appropriate model (i.e., compound **2**) is employed to determine the solution properties being used as a reference point for determining the effect of immobilization in monolayers. As was observed for **1**, irradiation at λ_{365} nm at 273 K results in a decrease in absorption at 350 nm and an increase at 253 nm corresponding to conversion from the *anti*-folded (**2A**) to the *syn*-folded (**2B**) conformational state (Figure 2). Warming to room temperature results in recovery of the original spectrum (**2A**). Conversion from **2A** to **2B** in the solid state (i.e., as thin films deposited on an ATR crystal) was confirmed by FTIR spectroscopy (Figure 2). Irradiation of **2A** at 365 nm results in a decrease in the intensity of the band of the ring breathing mode at the 1567 cm^{-1} and a blue shift of the band at 1457 cm^{-1} . The initial spectrum recovered after several minutes. Overall, changes to the FTIR spectrum upon irradiation are minor, as expected considering that only a change in conformation and not bonding is occurring. Nevertheless, the changes observed demonstrate the possibility of photoswitching between **2A** and **2B** in the solid state.

The cyclic voltammetry of **2A** in solution is shown in Figure 3a. The cyclic voltamogram shows that initially only **2A** is present in solution, that is, scanning initially from 0.7 V in a negative direction confirms the absence of **2²⁺**, which has a reduction potential of 0.36 V. On the return cycle toward positive potentials, an irreversible oxidation is observed at 1.21 V (vs SCE), which is accompanied on the subsequent scan toward negative potentials by an irreversible reduction wave at 0.36 V. The redox

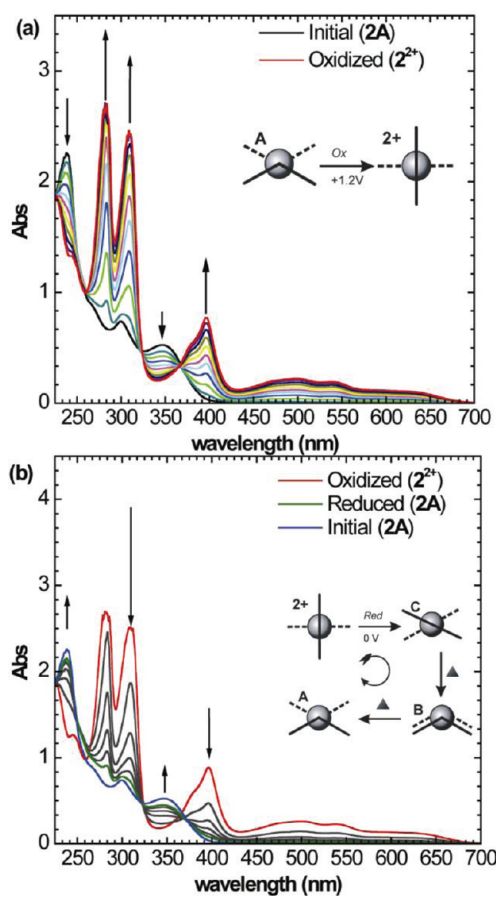


Figure 4. UV-vis spectroelectrochemistry (a) oxidation from **2A** to **2²⁺** at 1.2 V vs SCE and (b) reduction from **2²⁺** to **2A** at -0.3 V vs SCE.

behavior was found to be independent of the solvent/electrolyte combination employed (see, for example, Figure S5, SI) and is essentially the same as that observed for **1A** (Scheme 1).

UV-vis spectroelectrochemistry (Figure 4) shows the formation of **2²⁺** upon oxidation at 1.2 V and the full recovery of the initial spectrum of **2A** upon reduction at 0 V. In contrast to the methyl-substituted overcrowded alkene **1**, for **2** the UV-vis absorption spectrum of the dication is red-shifted and shows more clearly that the lowest energy absorption is a superposition of several distinct absorption bands. This is expected considering that the upper and lower halves are inequivalent due to the alkoxy substituent in the lower half of the molecule. Compound **2A** can be converted to the dicationic state (**2²⁺**) by preparative (bulk)electrolysis (and isolated as a PF₆⁻ salt, see SI, Figure S2). The cyclic voltammetry of **2²⁺** is similar to that of **2A**, with the reduction of **2²⁺** being observed at about 0.3 V and the current scaling with the square root of the scan rate (Figure 3b).

In contrast to the photochemical conversion of the *anti*-folded **2A** to the *syn*-folded **2B**, the oxidation of **2A** to **2²⁺** results in large changes in the FTIR (Figure 5a) and XPS spectra (Figure 5b) as well as in the UV-vis absorption spectrum. The changes in the FTIR spectrum are consistent with the large changes in structure that accompany oxidation. The S2p region of the XPS spectrum of the film of **2** contains only one doublet component at 163.6 eV, as expected for neutral sulfur atoms.²⁷ However, for a film of **2²⁺**, the major S2p component (70%) was at 165.1 eV and is assigned to the S¹⁺ oxidation state.²⁷ A minor component (ca. 15%

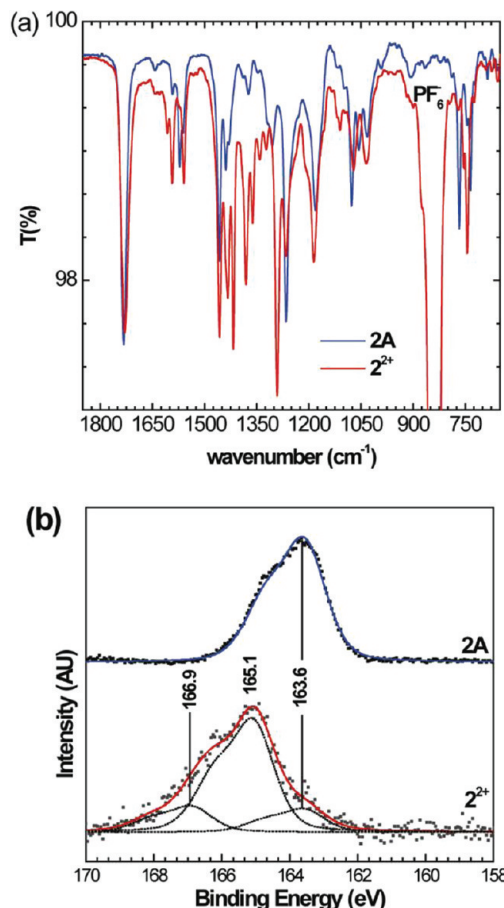


Figure 5. (a) Solid state FTIR spectra of **2A** and (**2²⁺**)(PF₆⁻)₂. (b) XPS data of the S2p core level region for **2A** and **2²⁺** as films on Au/mica.

assignable to the neutral form, **2** (S2p_{3/2} at 163.6 eV), is observed. The S2p_{3/2} peak of sulfur in a higher oxidation state was observed at 166.9 eV. Therefore, from the XPS measurements it is apparent that oxidation results in a considerable change (ca. 1.5 eV) in the binding energy of the sulfur 2p doublet, consistent with localization of the positive charge on the sulfur atoms, and relatively minor changes in the carbon region (see full spectrum, Figure S6, SI).

In summary, it can be concluded that, with respect to **1**, the introduction of the two alkoxy groups does not substantially perturb the basic photo- and electrochemistry of the overcrowded alkene.

Surface Functionalization by Self-Assembly of Switchable Molecules. Surfaces modified with self-assembled monolayers of **3** were characterized by ellipsometry, contact angle measurements, and XPS. The expected thickness of the SAM of **3**, composed of molecules perpendicularly oriented to a gold surface, is 1.75 nm. A thickness of 1.6 ± 0.05 nm was determined by ellipsometry, and from this it can be inferred that the molecules are tilted at 24° (±3°) with respect to the normal to the surface. Contact angle (CA) measurements with water gave values of 78° (±3°) for **3-Au** and 74° (±3°) for **4-ITO**, which when compared with bare Au (83 ± 3°) and ITO (30 ± 3°) are in agreement with the immobilization of **3** and **4** as monolayers on the respective surfaces.

Additional information on the composition of the monolayer and the bonding of the molecules to the surface was obtained by

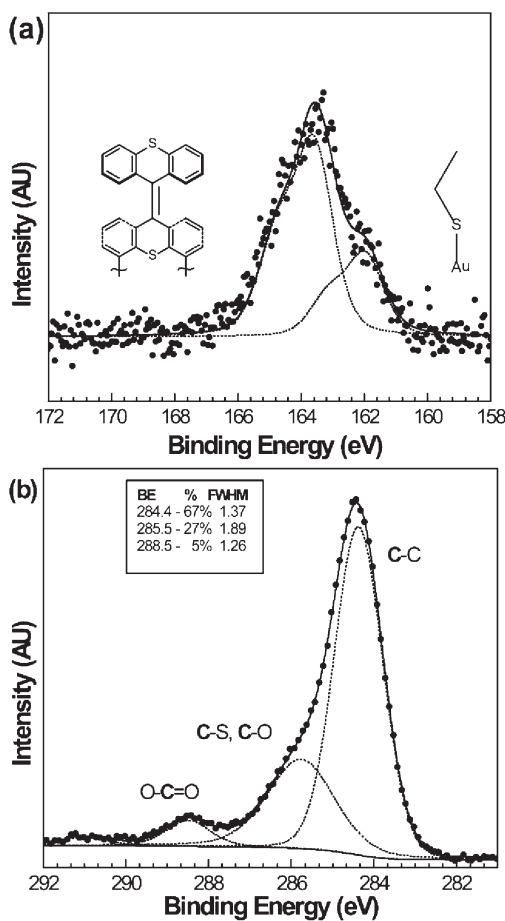


Figure 6. X-ray photoemission spectra of the S2p (a) and C1s (b) core level regions of 3-Au. Data and fits are shown (for details, see text). Inset: binding energies of the components, their full width at half-maximum (fwhm), and relative contribution.

XPS. A survey scan shows the fingerprint of the expected elements (S, C, O, Au) only. From the attenuated intensity of the gold photoelectron emission peak, the thickness of the molecular film was estimated to be 1.4 ± 0.1 nm, which is in agreement with the ellipsometry data and the theoretical length of the molecule. The spectra of the S2p and C1s core level regions are shown in Figure 6.

The sulfur 2p spectrum contains two contributions, one at a binding energy of 161.9 eV of the $2p_{3/2}$ level, corresponding to the S–Au bond, and another at 163.6 eV assigned to the sulfur bound to the carbon of the bisthianthrylidene part of the molecule.²⁸ The intensity ratio between these components $S_{\text{S}-\text{Au}}/S_{\text{S}-\text{C}}$, 33/67%, is in agreement with the expected attenuation of the S–Au component in a well-packed monolayer and implies formation of a monolayer only. Peaks at higher binding energy corresponding to oxidized species were not observed, as expected for a densely packed SAM of 3A.^{28a}

The overcrowded alkene (3-Au, Figure 1) consists of seven chemically inequivalent carbon atoms. The closely spaced peaks originating from C–O and C–S bonds can not be distinguished in the spectra; the same holds for aromatic and aliphatic carbon contributions. As a result, the peak at BE 284.4 eV is attributed to the aliphatic and aromatic parts (24 atoms) of the molecule accounting for 67% of the C1s signal.²⁹ The component at 285.8 eV corresponds to the 12 C–O, C–S bonds, which makes up 27.3%

of the carbon signal. The two carbonyl carbon atoms produce a peak at 288.5 eV and contribute 5.4% to the total C 1s signal. The satellite peak at 291 eV is assigned to $\pi-\pi^*$ shakeup of the aromatic parts of the molecule.³⁰

The carbon stoichiometry of the molecule gives a theoretical ratio between the intensities of the three spectral components as 24:12:2; experimentally a ratio 24.8:10:2 was found. The slightly lower contribution of the second component (C–O, C–S) can be rationalized by the attenuation of the two carbons bound to sulfur at the bottom (leg) position of the molecule and the neighboring carbon bonded to oxygen.

Taken together, ellipsometry, contact angle, and XPS spectroscopy confirm self-assembly of the overcrowded alkene switch as a densely packed monolayer on Au surfaces, attached via the sulfur legs, with an orientation tilted about 24° with respect to the surface normal.

Photochemistry of SAMs of 3 on Gold and Monolayers of 4 on Quartz. The UV/vis absorption spectrum of a monolayer of 4 assembled on quartz was measured to determine whether the photoinduced switching observed for 2 in solution (Figure 2a) was retained when immobilized on a solid surface. The UV/vis spectrum of 4-quartz shows absorption bands at about 230, 300, and 350 nm, in agreement with the spectrum of 2A. Irradiation of the modified quartz slide (4-quartz) at 365 nm for 30 min resulted in changes consistent with formation of the unstable *syn*-folded form 4B. The conversion is manifested in a decrease in absorbance at about 240 and 350 nm and an increase in absorbance at 260 nm (Figure 7), in agreement with the changes observed in the UV/vis absorption spectrum of 2 in solution (Figure 2a).

Due to the absorption of gold below 400 nm, monitoring of photochemical switching of a SAM of 3 on gold by UV/vis absorption spectroscopy is not feasible. However, formation of the unstable *syn*-folded form 3B from 3A by irradiation with UV light should lead to a decrease in intensity of the oxidation wave at 1.2 V and the appearance of a new broader oxidation wave at about 1.1 V as observed for 2A, and previously for 1A,⁷ in solution. Irradiation of SAMs of 3A on both gold slide and gold bead electrodes for 60 min at 365 nm, however, did not result in any change to the cyclic voltammetry (Figure 7, right). This result demonstrates that the SAM is stable even under prolonged UV irradiation.

Cyclic Voltammetry of SAMs of 3 and Monolayers of 4. SAMs of 3 and monolayers of 4 on electrode surfaces allow for electrochemically induced transformation of the switch to be induced and studied by cyclic voltammetry, in addition to the determination of surface coverage (Γ).³¹ The electrochemically determined surface coverage of 3 on a Au electrode was found to be $1.5 \times 10^{-10} \text{ mol cm}^{-2}$. The value obtained is consistent with monolayer formation, and is found to be independent of the concentration of the compound (in the range 10^{-4} – 10^{-7} M) in the solution from which self-assembly took place.³² In contrast for 4-ITO, the concentration of 4 in solution plays an important role in monolayer formation (Γ : 10^{-11} – $10^{-12} \text{ mol cm}^{-2}$), as a result of the kinetics of chemisorption and the irreversibility of the process. The monolayers formed on gold ($\Gamma = 10^{-10} \text{ mol cm}^{-2}$) are, in general, more dense than on ITO ($\Gamma = 10^{-11} \text{ mol cm}^{-2}$).

The redox behavior of both 3 and 4, when immobilized on a gold bead and on an ITO electrode, respectively, is shown in Figure 8. Even at low scan rates the cyclic voltammogram is stable over multiple cycles, indicating that oxidation to the dicationic state and the resulting increase in Coulombic repulsion between

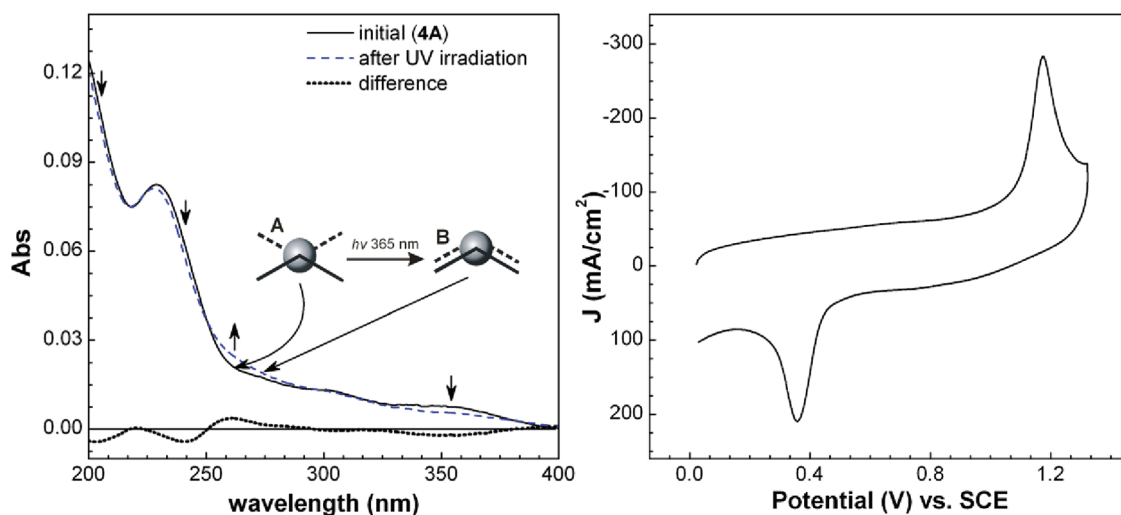


Figure 7. (a) UV/vis spectrum of 4-quartz: initial (solid line) and after irradiation at 365 nm (dashed line). A difference spectrum is shown in the bottom part of the graph (dotted line). Arrows indicate changes upon irradiation. (b) Cyclic voltammetry (0.1 V s^{-1}) in CH_2Cl_2 (0.1 M TBAPF₆) of a SAM of 3 on gold (on mica) after irradiation at 365 nm for 1 h (only first cycle is shown).

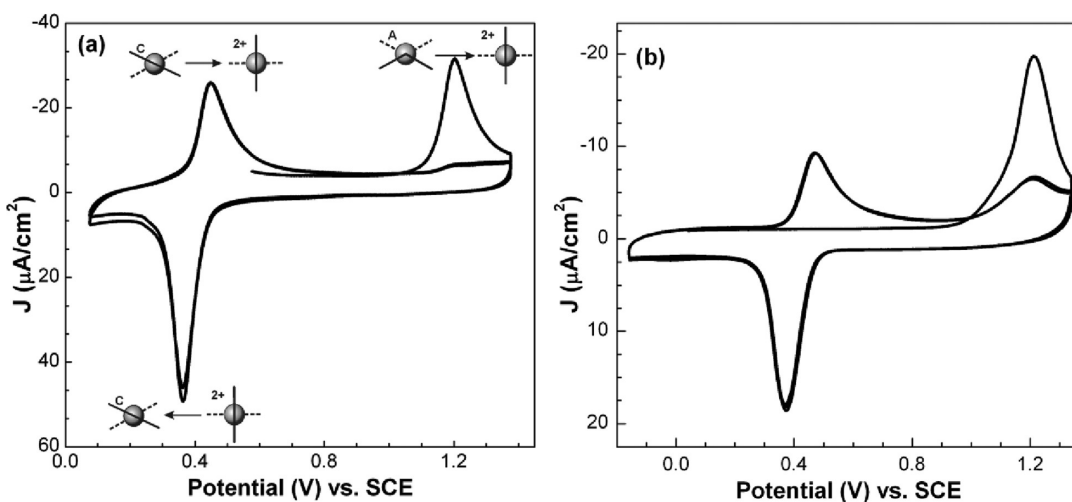


Figure 8. Cyclic voltammogram of 3-Au (a) and 4-ITO (b) in CH_2Cl_2 (0.1 M TBAPF₆) at 0.1 V s^{-1} .

molecules in the SAM is not sufficient to force desorption. The irreversible oxidation wave observed at 1.2 V in the first positive scan corresponds to the oxidation of the *anti*-folded form (3A, 4A) to the dicationic state (3^{2+} , 4^{2+}), as observed for 2A in solution (vide supra). On the return sweep toward negative potentials, a reduction wave is observed at 0.36 V, corresponding to the two electron reduction of the dicationic form, again as observed for 2A in solution. The relative intensity of each redox wave is independent of scan rate and shows the expected linear dependence of current on scan rate for a SAM (Figure 9). Remarkably on subsequent cycles the electrochemical behavior of 3 (and 4) on surfaces shows profound differences to that of 2 in solution.

In solution for both 1 and 2, the reduction of the dication (e.g., 2^{2+}) is irreversible at room temperature with thermal reversion of 2C (the twisted conformational state; see Scheme 1), which is formed initially upon reduction of 2^{2+} to 2A being much faster than the electrochemical time scale (Figures 3 and 4). In contrast, for both 3-Au and 4-ITO, the reversibility of the reduction of the dication to the neutral C form (Figure 9b, see twisted state;

Scheme 1, also) is substantial, as seen from the oxidation wave at about 0.4 V on the second cycle. It is possible that the increased reversibility of the reduction of the dication on surfaces is related to ion pairing effects; however, essentially the same behavior is observed (for the same SAM-coated bead electrode) in dichloromethane and in acetonitrile with several electrolytes (see SI, Figure S5). In the case of the 3-Au SAMs and 4-ITO monolayers, restoration of the *anti*-folded isomer is a thermally activated process and takes several minutes to achieve after one oxidation and reduction cycle of the SAM (Figure 10) in contrast to that observed in solution, where the thermal reversion is essentially instantaneous.

The electrochemical behavior of 3-Au and of 4-ITO are essentially the same, despite the difference in surface density and chemical nature of the surface attachment. Hence, the discussion focuses on 3-Au, but is applicable to both systems. The separation (ca. 0.85 V) between the oxidation and reduction waves reported previously for 1, and in the present study for 2, in solution is observed for 4-ITO and 3-Au also.

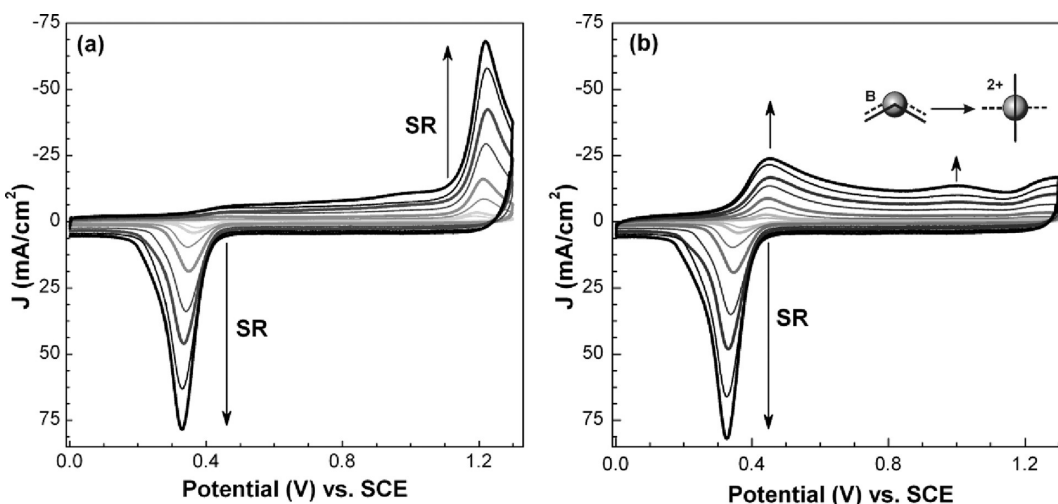


Figure 9. Scan-rate dependence of the cyclic voltammetry of the SAM 3-Au: (a) first cycle at each scan rate shown only and (b) second cycle at each scan rate. Scan rate varied from 0.1 to 5 V s^{-1} , 0.1 M TBAPF₆ in CH₂Cl₂. After each cycle, the bead was allowed to rest in electrolyte for 10 min.

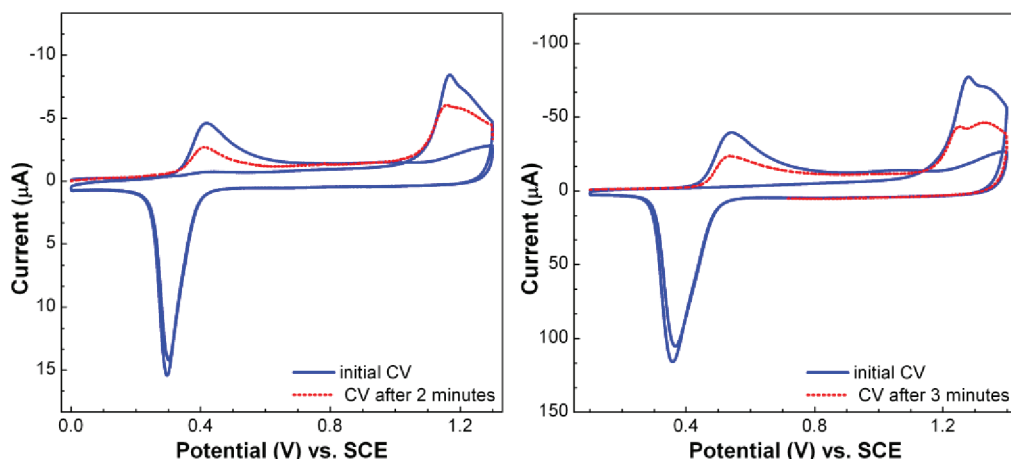


Figure 10. Recovery of the twisted neutral state 3C generated by reduction of 3²⁺. The initial cycle shown in blue oxidizes 3A to form 3²⁺, which is reduced on the return cycle. The potential was held at 0.0 V for two (left) and three (right) min before a second cycle commenced (red). The recovery of the anti-folded 3A is found to be incomplete with ca. 50% of the twisted form 3C still present (left, gold bead working electrode; right, Au on mica working electrode; scan rate 0.1 V s^{-1} , in CH₂Cl₂ with 0.1 M TBAPF₆).

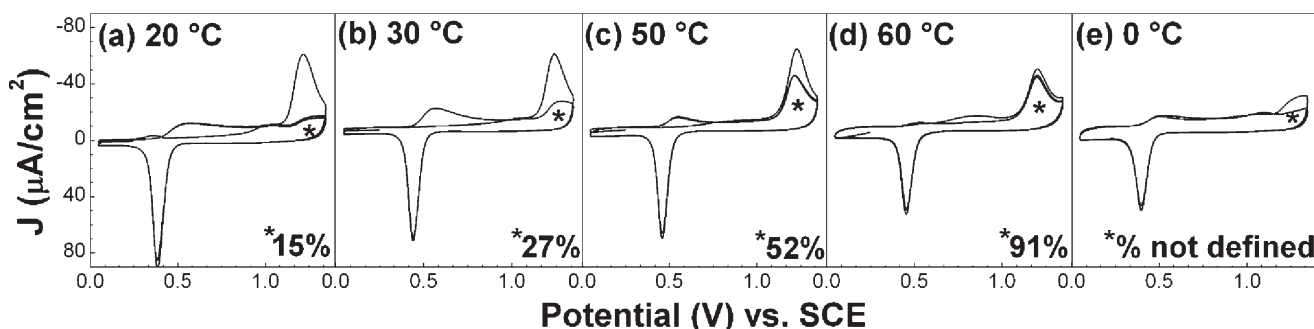


Figure 11. Temperature-dependence of the cyclic voltammetry of 3-Au. CVs at (a) 20, (b) 30, (c) 50, (d) 60, and (e) 0 °C; 0.1 M LiClO₄ in CH₃CN at 0.1 V s^{-1} .

The temperature-dependence of the cyclic voltammetry of a 3-Au SAM is shown in Figure 11. At all temperatures, the initial cycle shows oxidation of 3A to 3²⁺ at 1.2 V, followed by reduction

of 3²⁺ at about 0.4 V. At 20 °C, the redox wave associated with 3A on the second cycle is 15% of the intensity observed on the initial scan. As the temperature is increased, the recovery of 3A on the

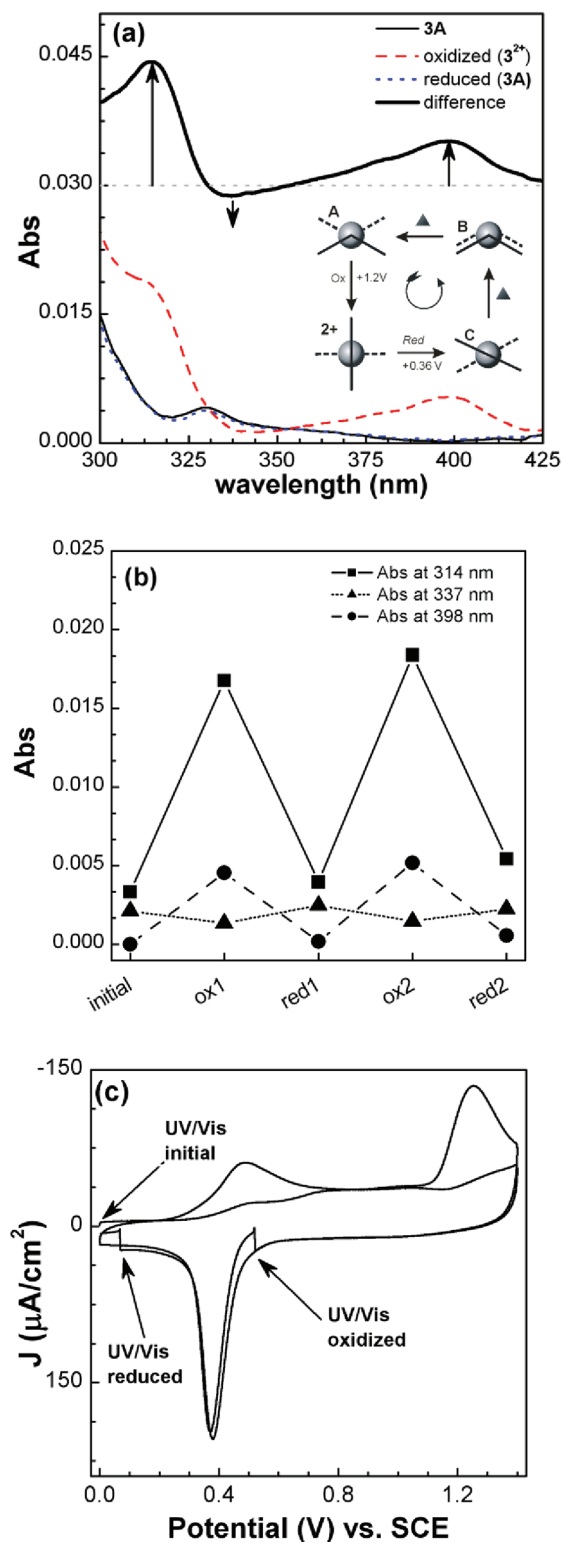


Figure 12. (a) UV/vis spectrum of the monolayer of 3 on a surface of 20 nm thin Au film on glass electrode during spectroelectrochemical oxidation (1.2 V) and reduction (0.0 V). The difference between the spectra of the initial and oxidized state is shown with an offset of +0.03. (b) Potential dependence of the intensities of individual absorption bands over several oxidation/reduction cycles. (c) Cyclic voltammetry in acetonitrile (0.1 M TBAPF₆) of the SAM of 3 on gold (on glass) recorded during spectroelectrochemistry (a), scan rate is 0.1 V s⁻¹.

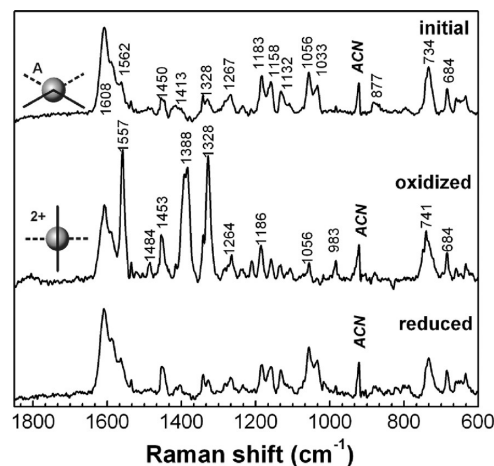


Figure 13. Surface-enhanced Raman (SERS) spectra of 3A-Au bead before and after oxidation and after subsequent reduction. A multipoint baseline correction has been applied to the spectra. The initial spectrum was recorded before applying a potential to the electrode. The spectrum *oxidized* was obtained after cycling the potential from 0 to 1.2 V and then to 0.6 V (vs SCE), that is, intermediate between the oxidation wave of 3A and the reduction wave of 3²⁺. The *reduced* spectrum was obtained by continuing the cyclic voltammogram from 0.6 to 0.0 V and holding the potential at 0.0 V.

time scale of the experiment (ca. 20 s between reduction of 3²⁺ at below 0.4 V and the reoxidation at 1.2 V) increases, and at 60 °C, the intensity in the second cycle reaches 90% that of the initial cycle. On returning the electrode to 0 °C, again 3A does not recover on the time scale of the cyclic voltammetry and the compound remains in the twisted and *syn*-folded states after reduction of 3²⁺-Au.

Importantly, although at elevated temperatures some desorption of 3-Au occurs with repeated cycling, manifested in a decrease in charge of the reduction wave of 3²⁺-Au, this decrease is only moderate and allows for extensive repeated measurements on each SAM-modified electrode. The % indicates the area of the oxidation wave (of 3A) on the second cycle with respect to the initial cycle.

UV/vis Absorption and Surface-Enhanced Raman Spectroelectrochemistry. UV/vis absorption spectroelectrochemistry was performed on SAMs of 3 on semitransparent Au slide electrodes (with a 20 nm thick layer of gold on glass). The absorption spectrum of 3-Au is characterized by a shoulder at about 300 nm ($\Gamma = 1.1 \times 10^{-10} \text{ mol cm}^{-2}$) and a maximum at 330 nm (Figure 12a). Oxidation at 1.2 V leads to substantial changes in the absorption spectrum consistent with the formation of 3²⁺-Au. Intense absorption bands appear at 314 and 398 nm, and a decrease in absorption is observed at 337 nm. The original spectrum can be recovered completely by reduction at 0.36 V and the oxidation and reduction could be repeated for several cycles, indicating that the SAM is stable in both oxidation states with respect to desorption (Figure 12b). The cyclic voltammogram of 3-Au on a transparent gold slide is shown in Figure 12c.

Surface-enhanced Raman spectroscopy was employed to study the oxidation and reduction of 3A on roughened gold bead electrodes. The Raman spectra of solid samples of 2A and 3A are shown in Figure S3 and show strong modes at 1610, 1586, 1563 cm⁻¹, as expected for an aromatic system. The initial spectrum of the SAM of 3A on roughened gold bead electrodes

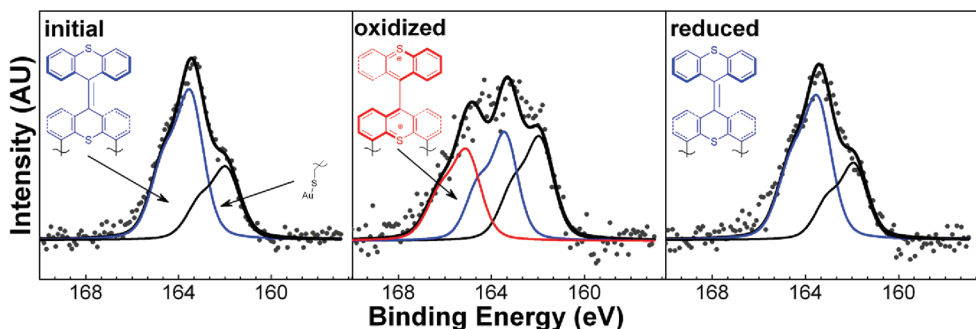


Figure 14. XPS spectra before and after oxidation to form a SAM of 3^{2+} and after subsequent reduction to reform the SAM of 3A on gold (on a mica substrate). Redox switching was carried out electrochemically in CH_2Cl_2 (0.1 M TBAPF₆).

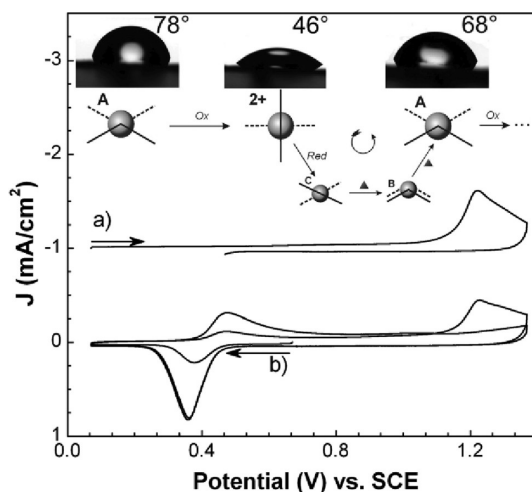


Figure 15. Change in contact angle of water on a SAM of 3-Au on mica before (left image) and after electrochemical oxidation (center image) and subsequent reduction (right image) in CH_2Cl_2 (0.1 M TBAPF₆). The corresponding cyclic voltammograms (scan rate 0.1 V s^{-1}) are shown below the droplet images.

(Figure 13, top) contains aromatic ring breathing modes at 1608 , 1586 , and 1562 cm^{-1} , consistent with the solid state spectrum of 3A . Upon oxidation at 1.2 V a large change in the SERS spectrum was observed with the appearance of four strong modes at 1557 , 1453 , 1388 , 1328 cm^{-1} (Figure 13, middle). Reduction again at 0.0 V resulted in a recovery of the initial spectrum (Figure 13, bottom).

X-ray Photoelectron Spectroscopy and Contact Angles of Oxidized SAMs. The XPS spectrum of a SAM of 3A on a gold film (on mica) shows a pattern of changes upon electrochemical oxidation (Figure 14), consistent with those measured on a thin film of 2^{2+} (vide supra) with new components in the $S2p$ core level region due to the sulfur chemisorbed to the gold surface. The chemisorbed sulfur component (33%) remains unaffected by electrochemical oxidation (Figure 14, center). However, the intensity of the bisthianthylidene sulfur peak at 163.6 eV decreased due to electrochemical conversion to the dicationic state, which results in a line shifted to 165.0 eV . The cyclic voltammogram of the 3A on gold coated mica slide used for XPS measurements is identical to that shown in Figure 15. Subsequent reduction of the electrochemically oxidized SAM results in a complete recovery of the original XPS spectrum of 3A-Au and a complete absence of signals from PF_6^- , as expected for the

neutral state. In addition, this indicates that the monolayer is stable in the oxidized state for at least several hours and under the vacuum conditions of the XPS instrument.

Electrochemical oxidation to the dicationic form 3^{2+} -Au manifests itself in a change in the contact angle of water on the surface of the SAM (Figure 15). The oxidized SAM is less hydrophobic and the contact angle decreases to 46° ($\pm 3^\circ$) from an initial value of 78° ($\pm 3^\circ$). This change is reversed upon reduction with the contact angle restored to 68° ($\pm 3^\circ$). The process was repeatable for several cycles.

The changes in contact angle are unlikely to be due to changes in molecular structure, that is, *anti*-folded versus orthogonal. It is more reasonable to ascribe the changes in contact angle to changes in polarity, especially when the differences in solubility between 2A and $2^{2+}(\text{PF}_6^-)_2$ are considered. Compound 2A is soluble in CH_2Cl_2 but only sparingly soluble in CH_3CN , while $2^{2+}(\text{PF}_6^-)_2$ is soluble in CH_3CN , but only sparingly in CH_2Cl_2 . Hence, in the reduced state, the surface should be more hydrophobic than in the oxidized state, which is observed (Figure 15).

CONCLUSIONS

In the present contribution, the effect of immobilization of analogs of 2A on a range of surfaces was investigated with regard to changes in electrochemical, thermal, and photochemical behavior. Modification of the overcrowded alkene with thiol- or alkylsiloxy-terminated aliphatic “legs” enabled immobilization of the overcrowded alkenes (3A and 4A) on gold, quartz, and ITO. The SAMs and monolayers formed have been characterized by XPS, UV/vis absorption, and surface-enhanced Raman spectroscopy as well as electrochemically. Overall, the properties of 2A were found to be retained when immobilized on surfaces. However, whereas in solution intermolecular interactions are essentially absent, when immobilized on surfaces both as SAMs and as monolayers, intermolecular interactions dominate the thermal and photochemical properties. With regard to photochemical activity a combination of rapid intermolecular excited state deactivation (as seen for related SAMs earlier)¹⁵ and the tight packing within the monolayers serves to reduce the efficiency of the *anti/syn*-isomerization. The ability to access highly unstable states by electrochemical oxidation in the present system allows for the effect of packing on thermal relaxation to the lowest energy conformer (the *anti*-folded state) to be observed. Remarkably, whereas in solution the twisted conformer, which lies 18 kcal mol^{-1} above the *anti*-folded state,¹³ is not observable, it is stable for several minutes at room temperature after being formed by

reduction of a SAM of 3^{2+} on gold. The results described here underline the need to consider the increase in the contribution of intermolecular interactions in densely packed arrangements when designing functional surfaces based on SAMs of photo/electrochromic molecular systems, which undergo large structural changes in response to external stimuli, in particular, electrochemistry. The large hysteresis and volatile memory, that is, the slow reversion of the highly unstable twisted conformation to the *anti*-folded conformation, opens new prospects in organic electronics.

■ ASSOCIATED CONTENT

S Supporting Information. Details of synthesis and characterization, FTIR, Raman, and XPS spectra, electrochemistry, and procedures for preparation of substrates. This material is available free of charge via the Internet at <http://pubs.acs.org>.

■ AUTHOR INFORMATION

Corresponding Author

E-mail: b.l.feringa@rug.nl; p.rudolf@rug.nl; w.r.browne@rug.nl

■ ACKNOWLEDGMENT

This work was performed within MSC^{plus} program of the Zernike Institute for Advanced Materials and received additional support from the “Stichting voor Fundamenteel Onderzoek der Materie (FOM)”, which is financially supported by The Netherlands Organisation for Scientific Research (NWO), and NWO-CW (VIDI Grant 700.57.428, H.L. and W.R.B.), NanoNed (P.V.W., B.L.F.), and the European Research Council (B.L.F., ERC Grant No. 227897).

■ REFERENCES

- (a) Woll, C. *Angew. Chem., Int. Ed.* **2009**, *48*, 8406–8408.
- (b) Browne, W. R.; Feringa, B. L. *Annu. Rev. Phys. Chem.* **2009**, *60*, 407–428. (c) Fox, M. A. *Acc. Chem. Res.* **1999**, *32*, 201–207.
- (a) Aviram, A.; Ratner, M. A. *Chem. Phys. Lett.* **1974**, *29*, 277–283. (b) Green, J. E.; Choi, J. W.; Boukai, A.; Bunimovich, Y.; Johnston-Halperin, E.; Delonno, E.; Luo, Y.; Sheriff, B. A.; Xu, K.; Shin, Y. S.; Tseng, H.; Stoddart, J. F.; Heath, J. R. *Nature* **2007**, *445*, 414–417.
- (c) Kronemeijer, A. J.; Akkerman, H. B.; Kudernac, T.; van Wees, B. J.; Feringa, B. L.; Blom, P. W. M.; de Boer, B. *Adv. Mater.* **2008**, *20*, 1467–1473.
- (3) Simao, C.; Mas-Torrent, M.; Crivillers, N.; Lloveras, V.; Artes, J. M.; Gorostiza, P.; Veciana, J.; Rovira, C. *Nat. Chem.* **2011**, *3*, 359–364.
- (4) de Silva, A. P.; Uchiyama, S. *Nat. Nanotechnol.* **2007**, *2*, 399–410.
- (5) (a) Mendes, P. M. *Chem. Soc. Rev.* **2008**, *37*, 2512–2529. (b) Robertus, J.; Browne, W. R.; Feringa, B. L. *Chem. Soc. Rev.* **2010**, *39*, 354–378.
- (6) Hauser, A. *Top. Curr. Chem.* **2004**, *234*, 155–198.
- (7) Browne, W. R.; Pollard, M. M.; de Lange, B.; Meetsma, A.; Feringa, B. L. *J. Am. Chem. Soc.* **2006**, *128*, 12412–12413.
- (8) (a) Mills, N. S.; Levy, A.; Plummer, B. F. *J. Org. Chem.* **2004**, *69*, 6623–6633. (b) Malandra, J. L.; Mills, N. S.; Kadlecak, D. E.; Lowery, J. A. *J. Am. Chem. Soc.* **1994**, *116*, 11622–11623. (c) Mills, N. S.; Malandra, J. L.; Burns, E. E.; Green, A.; Unruh, K. E.; Kadlecak, D. E.; Lowery, J. A. *J. Org. Chem.* **1997**, *62*, 9318–9322. (d) Mills, N. S.; Burns, E. E.; Hodges, J.; Gibbs, J.; Esparza, E.; Malandra, J. L.; Koch, J. *J. Org. Chem.* **1998**, *63*, 3017–3022. (e) Mills, N. S.; Benish, M. A.; Ybarra, C. *J. Org. Chem.* **2002**, *67*, 2003–2012. (f) Mills, N. S. *J. Am. Chem. Soc.* **1999**, *121*, 11690–11696.
- (9) (a) Schonberg, A.; Ismail, A. F. A.; Asker, W. *J. Chem. Soc.* **1946**, 442–446. (b) Schonberg, A.; Mustafa, A.; Sobhy, M. E. *J. Am. Chem. Soc.* **1953**, *75*, 3377–3378. (c) Korenstein, R.; Muszkat, K. A.; Fischer, E. *J. Photochem.* **1976**, *5*, 447–456. (d) Biedermann, P. U.; Stezowski, J. J.; Agranat, I. *Eur. J. Org. Chem.* **2001**, 15–34. (e) Korenstein, R.; Muszkat, K. A.; Sharafy-Ozeri, S. *J. Am. Chem. Soc.* **1973**, *95*, 6177–6181. (f) Fanselow, D. L.; Drickamer, H. G. *J. Chem. Phys.* **1974**, *61*, 4567–4573. (g) Agranat, I.; Tapuhi, Y. *J. Am. Chem. Soc.* **1976**, *98*, 615–616. (10) Mayer, F. *Ber. Dtsch. Chem. Gesell.* **1909**, *42*, 1132–1137.
- (11) (a) Rabinovitz, M.; Agranat, I.; Weitzen-Dagan, A. *Tetrahedron Lett.* **1974**, *15*, 1241–1244. (b) Brunetti, F. G.; Gong, X.; Tong, M.; Heeger, A. J.; Wudl, F. *Angew. Chem., Int. Ed.* **2010**, *49*, 532–536. (c) Levy, A.; Biedermann, P. U.; Cohen, S.; Agranat, I. *J. Chem. Soc., Perkin Trans. 2* **2001**, 2329–2341.
- (12) (a) Feringa, B.; Wynberg, H. *J. Am. Chem. Soc.* **1977**, *99*, 602–603. (b) Koumura, N.; Zijlstra, R. W. J.; van Delden, R. A.; Harada, N.; Feringa, B. L. *Nature* **1999**, *401*, 152–155. (c) Koumura, N.; Geertsema, E. M.; van Gelder, M. B.; Meetsma, A.; Feringa, B. L. *J. Am. Chem. Soc.* **2002**, *124*, 5037–5051. (d) van Delden, R. A.; ter Wiel, M. K. J.; Pollard, M. M.; Vicario, J.; Koumura, N.; Feringa, B. L. *Nature* **2005**, *437*, 1337–1340.
- (13) (a) Biedermann, P. U.; Stezowski, J. J.; Agranat, I. *Eur. J. Org. Chem.* **2001**, 15–34. (b) Bowyer, W. J.; Engelman, E. E.; Evans, D. H. *J. Electroanal. Chem.* **1989**, *262*, 67–82.
- (14) Feringa, B.; Wynberg, H. *J. Am. Chem. Soc.* **1977**, *99*, 602–603.
- (15) Coleman, A. C.; Areephong, J.; Vicario, J.; Meetsma, A.; Browne, W. R.; Feringa, B. L. *Angew. Chem., Int. Ed.* **2010**, *49*, 6580–6584.
- (16) Similar photocyclization is observed for **1A** only after prolonged irradiation.
- (17) Areephong, J.; Browne, W. R.; Katsonis, N.; Feringa, B. L. *Chem. Commun.* **2006**, 3930–3932.
- (18) Dirama, T. E.; Johnson, J. A. *Langmuir* **2007**, *23*, 12208–12216.
- (19) London, G.; Carroll, G. T.; Fernández Landaluce, T.; Pollard, M. M.; Rudolf, P.; Feringa, B. L. *Chem. Commun.* **2009**, 1712–1714.
- (20) Valkenier, H.; Huisman, E. H.; van Hal, P. A.; de Leeuw, D. M.; Chiechi, R. C.; Hummelen, J. C. *J. Am. Chem. Soc.* **2011**, *133*, 4930–4939.
- (21) Duwez, A.-S. *J. Electron Spectrosc. Relat. Phenom.* **2004**, *134*, 97–138.
- (22) LISE laboratory of the Facultés Universitaires Notre-Dame de la Paix, Namur, Belgium.
- (23) Moulder, J. F.; Stickle, W. F.; Sobol, P. E. *Handbook of X-ray Photoelectron Spectroscopy*; Perkin-Elmer, Physical Electronics Division: Eden Prairie, MN, 1993.
- (24) Shirley, D. A. *Phys. Rev. B* **1972**, *5*, 4709–4714.
- (25) Lamont, C. L. A.; Wilkes, J. *Langmuir* **1999**, *15*, 2037–2042.
- (26) In temperature-dependent studies, CH_3CN with 0.1 M LiClO_4 was used as an electrolyte.
- (27) Lindberg, B. J.; Hamrin, K.; Johansson, G.; Gelius, U.; Fahlman, A.; Nordling, C.; Siegbahn, K. *Phys. Scr.* **1970**, *1*, 286–298.
- (28) (a) Nuzzo, R. G.; Zegarski, B. R.; Dubois, L. H. *J. Am. Chem. Soc.* **1987**, *109*, 733–740. (b) Mendoza, S. M.; Berná, J.; Pérez, E. M.; Kay, E. R.; Mateo-Alonso, A.; De Nadaï, C.; Zhang, S.; Baggerman, J.; Wiering, P. G.; Leigh, D. A.; Prato, M.; Brouwer, A. M.; Rudolf, P. *J. Electron Spectrosc. Relat. Phenom.* **2008**, *165*, 42–45. (c) Castner, D. G.; Hinds, K.; Grainger, D. W. *Langmuir* **1996**, *12*, 5083–5086. (d) Bain, C. D.; Troughton, E. B.; Tao, Y. T.; Evall, J.; Whitesides, G. M.; Nuzzo, R. G. *J. Am. Chem. Soc.* **1989**, *111*, 321–335.
- (29) Gelius, U.; Hedén, P. F.; Hedman, J.; Lindberg, B. J.; Manne, R.; Nordberg, R.; Nordling, C.; Siegbahn, K. *Phys. Scr.* **1970**, *2*, 70–80.
- (30) Gelius, U. *Phys. Scr.* **1974**, *9*, 133–147.
- (31) (a) Markovich, I.; Mandler, D. *Analyst* **2001**, *126*, 1850–1856. (b) Eckermann, A. L.; Feld, D. J.; Shaw, J. A.; Meade, T. J. *Coord. Chem. Rev.* **2010**, *254*, 1769–1802. (c) García-Raya, D.; Madueño, R.; Blázquez, M.; Pineda, T. *J. Phys. Chem. C* **2010**, *114*, 3568–3574. (d) Browne, W. R.; Kudernac, T.; Katsonis, N.; Areephong, J.; Hjelm, J.; Feringa, B. L. *J. Phys. Chem. C* **2008**, *112*, 1183–1190.
- (32) The SAMs formed result in the capacitance of the electrode changing from $20 \mu\text{F cm}^{-2}$ for an unmodified Au electrode to $4 \mu\text{F cm}^{-2}$ for 3-Au.